



HAL
open science

Design and performance of the MICADO high contrast mode

Pierre Baudoz, Elsa Huby, Fabrice Vidal, Eric Gendron, Yann Clenet, Ric Davies

► **To cite this version:**

Pierre Baudoz, Elsa Huby, Fabrice Vidal, Eric Gendron, Yann Clenet, et al.. Design and performance of the MICADO high contrast mode. Adaptive Optics for Extremely Large Telescopes 7th Edition, ONERA, Jun 2023, Avignon, France. 10.13009/AO4ELT7-2023-092 . hal-04402841

HAL Id: hal-04402841

<https://hal.science/hal-04402841>

Submitted on 18 Jan 2024

HAL is a multi-disciplinary open access archive for the deposit and dissemination of scientific research documents, whether they are published or not. The documents may come from teaching and research institutions in France or abroad, or from public or private research centers.

L'archive ouverte pluridisciplinaire **HAL**, est destinée au dépôt et à la diffusion de documents scientifiques de niveau recherche, publiés ou non, émanant des établissements d'enseignement et de recherche français ou étrangers, des laboratoires publics ou privés.



Design and performance of the MICADO high contrast mode

Pierre Baudoz^a, Elsa Huby^a, Fabrice Vidal^a, Eric Gendron^a, Yann Clénet^a, and
Richard Davies^b

^aLESIA, Observatoire de Paris, Université PSL, CNRS, Sorbonne Université,
Université Paris Cité, Meudon, France

^bMax-Planck-Institut für extraterrestrische Physik, Garching, Germany

ABSTRACT

MICADO will be the first-light near-infrared imager of the European Extremely Large Telescope (ELT). MICADO will be equipped with a high contrast imaging mode dedicated to the observation and characterization of exoplanets and planetary systems. The increase in sensitivity and angular resolution between the current high contrast instruments like SPHERE on the VLT or GPI on GEMINI and MICADO will allow a quantitative and qualitative jump on the study of these planetary systems. MICADO will be equipped with a set of three classical Lyot coronagraphs, one phase-apodized pupil coronagraph and two sparse aperture masks. These components are optimized for different observing conditions in narrow or large spectral band between 1150 nm and 2300 nm and will rely on the well-corrected point spread function delivered by the Single Conjugate Adaptive Optics (SCAO) of MICADO.

In this paper, we describe the final design of the MICADO high contrast mode, explain the reasons that led to the choice of 3 classical Lyot coronagraphs and give the expected performance of these coronagraphs for different atmospheric conditions.

Keywords: MICADO, high contrast imaging, vortex, classical Lyot coronagraph

1. INTRODUCTION

Instruments using extreme adaptive optics, such as SPHERE on the VLT [1] and GPI on GEMINI [8], have significantly advanced our comprehension of planetary system formation and evolution. Nonetheless, several questions remain unanswered, including those concerning formation scenarios, planetary atmospheres, the frequency of giant planets in distant orbits exceeding 5-10 AU, and more. While space instruments on board the JWST will offer fresh insights into exoplanetary science, they are constrained in terms of contrast and angular resolution when compared to an instrument designed for use on the ELT. The building of a specialized instrument for direct imaging and spectroscopy of exoplanets on the ELT like ESO's Planetary Camera and Spectrograph (PCS) will only occur after the initial instruments are commissioned. Exploiting the 5-fold improvement in angular resolution between the ELT and current ground-based or planned space-based telescopes presents an opportunity for exoplanetary research prior to the anticipated deployment of the dedicated ELT planet finders in the middle to late 2030s

2. KEY ELEMENTS OF THE HIGH CONTRAST MODE

The elements of the high contrast imaging mode are described below and their respective main features are detailed in Table 1.

Coronagraph	IWA or equivalent	Spectral bands	Notes
CLC0	15 mas	J & H only	limited zenith angle
CLC1	25 mas	J to K	limited zenith angle
CLC2	50 mas	J to K	
vAPP	2.6 λ/D	J to K	only narrow band & OWA= 20 λ/D
SAM1	0.5 λ/D	J to K	9 holes
SAM2	0.5 λ/D	J to K	12 holes

Table 1. Summary of the different high-contrast imaging modes

Unlike SPHERE, MICADO is not exclusively oriented towards exoplanet science. Consequently, the optical design of MICADO represents a compromise between all the modes of the instrument. The key elements of MICADO high-contrast mode are detailed below.

2.1 Classical Lyot Coronagraphs

The basic concept of coronagraphy was introduced by B. Lyot in the 1930's for solar application [7]. Since that time, the concept has evolved to stellar application but has remained quite similar. The primary goal is to observe faint objects (point source or extended) near bright ones. However, stellar coronagraphy strongly differs from solar coronagraphy since the central source is actually point-like thus providing a diffraction pattern which dominates the environment. A stellar coronagraph is therefore a starlight suppression device designed to reduce the diffracted starlight as much as possible.

In its basic concept, an amplitude mask, the so-called Lyot mask, is placed in the focal plane to block the central part of the image. However, it was identified by B. Lyot that the combination with a diaphragm located in the subsequent pupil was mandatory, the so-called Lyot stop. Indeed, when the Lyot mask blocks part of the diffracted Point Spread Function (PSF) of the telescope, the light distribution in the downstream pupil is quite different from the one in the input pupil. Instead of a uniform distribution inside the geometric aperture, the light is mostly diffracted on the edge of the pupil. The action of the Lyot stop is precisely to select a smaller part of the pupil in which the on-axis starlight is rejected. After the Lyot stop, an image of the field can be formed with the starlight attenuated. On the contrary, an off-axis object missing the central opaque mask has its pupil unaltered and is re-imaged in the final detector plane. The actual situation is more complex since telescopes are usually centrally obstructed and because the light is propagating through the atmosphere. Even if an AO system is in used, residual phase aberrations (corresponding to high spatial frequency patterns) are also missing the focal mask and are therefore found in the final image. The performance of a coronagraph including phase aberrations, non-circular aperture and other limitations can be accurately modeled with numerical simulations.

Because of its large central obscuration and its segmented pupil, the ELT pupil is not optimized for coronagraphy. Indeed, the large central obscuration and the presence of gaps increase the number of edges in the pupil, thus the amount of stellar light diffracted by these edges. One solution to overcome this problem is to couple the focal plane mask with an apodization mask at the entrance pupil of the instrument to compensate for the effect of the diffraction by the central obscuration. However, the final design of MICADO does not permit it. In this context, simple Classical Lyot Coronagraphs (CLC), without apodization are selected as a baseline for MICADO. A CLC is an occulting mask in the focal plane and must be coupled with a Lyot stop located in a pupil plane downstream of the focal plane mask.

2.1.1 CLC1

To take full advantage of the high angular resolution of the ELT, we decided to select one CLC that allows the detection of planet at short distance from the star (coronagraph with a small Inner Working Angle, IWA). The selection of the size of the focal plane masks is linked to the selection of the dimension of the Lyot stop. The sizes of the 2 elements (radius of the focal mask and filtering of the Lyot stop) are optimized at the same time for

both CLC1 and CLC2 (see below). The final radius of CLC1 is 25 milliarcseconds (mas), corresponding to $2 \lambda/D$ at the wavelength of $2.2 \mu\text{m}$. For more information on this optimization, see [10].

2.1.2 CLC2

In MICADO, the Atmospheric Dispersion Compensator (ADC) will be placed after the entrance focal plane where we put the focal plane masks. This will limit the use of CLC1 to narrow spectral bandwidth at large zenith angle. A second CLC is optimized with a medium IWA ($4\text{-}5 \lambda/D$) to take care of the PSF elongated by the atmospheric dispersion, especially with broadband filter while ensuring a good sensitivity of the coronagraphic mode. The CLC2 mask has a radius of 50 mas.

The Lyot stop shape and the focal plane mask radius were jointly optimized for both CLC1 and CLC2. The same specifications were found for the Lyot stop, resulting in a diaphragm with an outer radius undersized by 14% with respect to the telescope radius, and an oversized central obscuration of 36%, leading to a final transmission of 61%.

Three Lyot stops are actually included in MICADO to block the stellar light diffracted by the mask. These Lyot stops have an identical shape but 2 of them are coupled with Neutral density filters to allow photometric calibration of bright stars when they are moved outside of the coronagraphic mask. The transmissions of these 3 stops are respectively : 61%, 6%, 0.06% allowing calibration up to magnitude $K=3$ without saturating the detector.

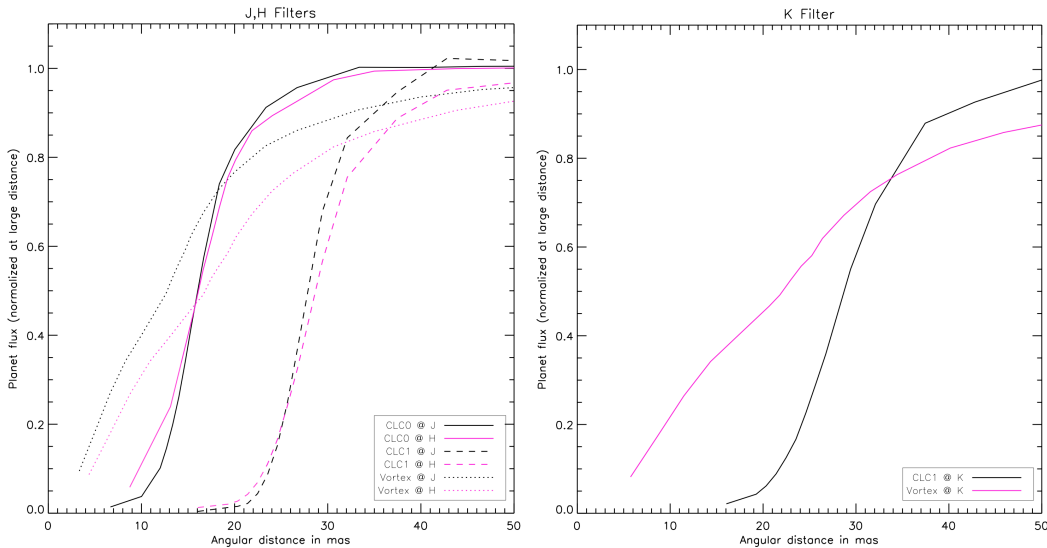


Figure 1. Left: Transmission as a function of angular separation for CLC0, CLC1 and a vortex for J and H band. Right: Transmission as a function of angular separation for CLC1 and a vortex for K band. All coronagraphs have the same Lyot stop. Transmission is normalized at large distance from the coronagraph axis.

2.1.3 CLC0 or vortex?

We also studied the improvement when adding a more complex coronagraph like a vortex coronagraph [9] to allow reaching even smaller angular separation to the star in J-H bands ($2 \lambda/D : 10\text{-}15 \text{ mas}$). As the CLC, a vortex coronagraph requires a focal plane mask and a Lyot stop. In the focal plane, it is a phase mask which has a shape of an azimuthal phase ramp that varies from 0 to $2l_p\pi$ with l_p the topological charge of the vortex. We simulated charge 2 and charge 4 vortex coronagraphs. Both solutions are very sensitive to central obscuration and would require a Lyot stop filtering much more than 60% of the incoming light. A charge 4 vortex will have an Inner Working Angle (IWA) of $4 \lambda/D$ (transmission = 50% @ $4 \lambda/D$ and dropping rapidly closer in), preventing from detection at short angular distance. Thus, we only compare the performance of charge 2 vortex coronagraphs with CLC1 and CLC0, a Classical Lyot Coronagraph made of a focal plane mask with a 15 mas radius. All coronagraphs use the same Lyot stop defined above.

First, we compare the IWA of a charge 2 vortex (assuming the vortex is perfectly achromatic) with the IWA of CLC0 and CLC1. As shown in Figure 1 (left), the transmission of an off-axis source (an exoplanet for example) is better with CLC0 at separation >16 mas (>18 mas) in J band (H band). CLC0 is not compatible with filters in the K band since the mask radius is only $1.3\lambda/D$, preventing the attenuation of the star. For this spectral band, we compare the performance of a vortex with CLC1 (Figure 1, right). At K band, a vortex would have a marginal improvement between 20 and 33mas. However, since the vortex has a better transmission at small angular distance, it is also more sensitive to residual tip-tilt uncorrected by the AO. Thus residual low-order aberration speckles are a limiting factor for a vortex when looking for faint point source object at short angular distance as shown in Figure 2.

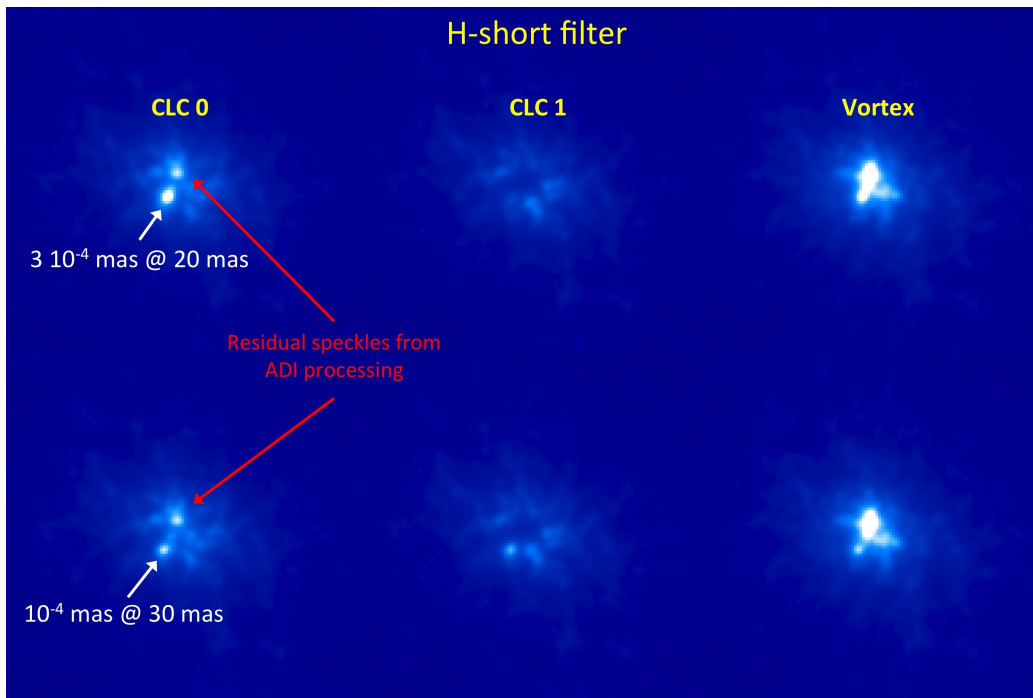


Figure 2. ADI Post-processing of two faint objects close to the star for CLC0, CLC1 and a vortex. Simulations inputs defined Section 3 with AO corrected residual turbulence averaged over 30s (120 images sampled @ 1 Hz), median seeing and no NCPA.

Another interesting science target of the CLC0 is the imaging of small debris disks. As shown in Figure 3, CLC0 does not attenuate the disk more than the vortex in J and H. In K, the CLC1 has roughly the same effect as the vortex. Thus, the vortex is discarded because it is too sensitive to residual atmospheric jitter and is not really more sensitive than CLC0 in J and H and CLC1 in K.

2.2 Phase apodization Pupil plane mask

As already said above, correction of atmospheric dispersion can only be applied downstream of the focal plane coronagraph which limits the detection at short separation and large zenith angle. One solution is to use pupil plane components like phase or amplitude apodization that are less sensitive to jitter and will be located after the ADC, thus will not be limited by atmospheric dispersion.

A pupil phase apodization uses interferences to attenuate the diffraction wings in a limited area of the field of view, called Dark Hole, without decreasing the total transmission of the instrument. This apodization decreases the Strehl ratio (SR) and an optimization needs to be done to maximize the SR and the useful FOV while minimizing the diffracted light at the shortest angular separation. In MICADO, we choose a vector Apodizing Phase Plate (vAPP, [11, 3]). The vAPP can be designed for any pupil geometry even though complex pupil

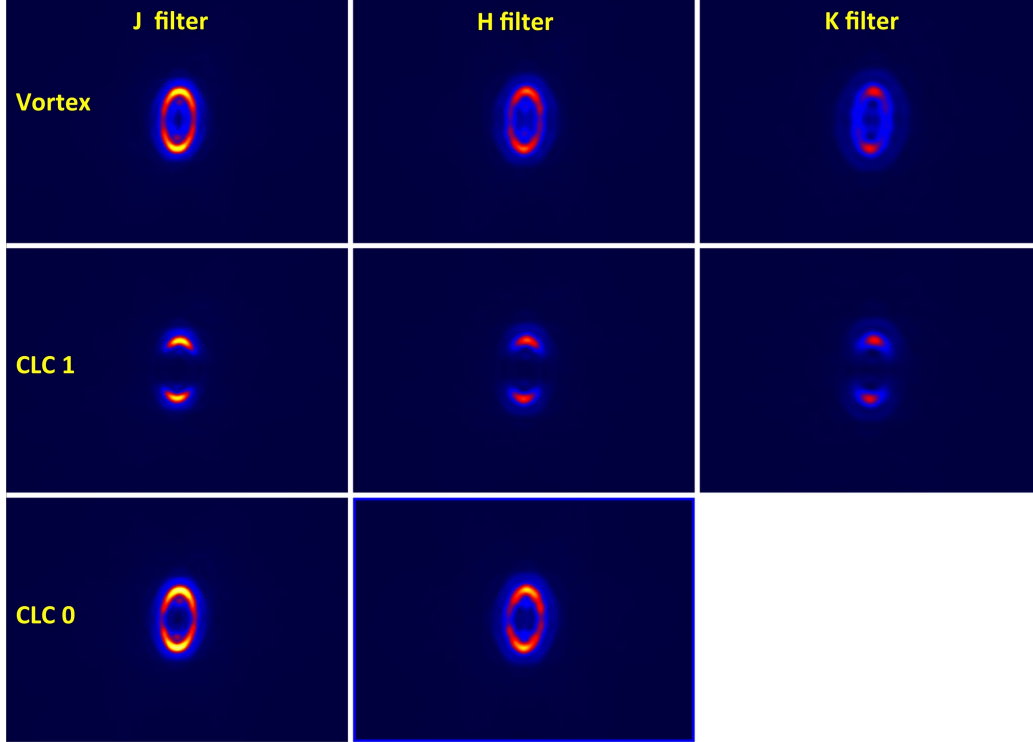


Figure 3. Coronagraph attenuation for a 4AU disk around star at 116 pc (34 mas size for the longest direction and 58° inclination). The stellar distance corresponds to HD141569 where a disk is observed with the same 58° inclination but 12 times further at 48 AU.

structure might decrease the Strehl ratio when trying to reach short angular separation. The vAPP that will be located in the pupil wheel of MICADO is designed with the following main characteristics:

- Rectangular shape Dark hole
- Inner Working Angle of $2.6 \lambda/D$
- Outer Working Angle of $20 \lambda/D$
- Theoretical contrast @ $3\lambda/D$ without aberrations: 10^{-4}

2.3 Sparse Aperture Masks

MICADO will also include two Sparse Aperture Masks (SAM). The principle of SAM is to insert in the pupil an opaque mask with a number of holes spatially distributed so that each pair of holes will contribute to a unique spatial frequency. Thus SAM imaging mode avoids the combinations of multiple spatial frequencies which – adding incoherently – may degrade the transfer function. With a well known transfer function of the instrument, one can partly distinguish the effect of optical aberrations from astronomical information and retrieve more precisely the environment of the star at very short angular separation [5]. The design of the SAM masks are not completely final but should include a 9-hole mask with $\approx 3\text{m}$ diameter holes allowing a total collecting area of 63 m^2 greater than the surface of a single VLT unit telescope. The second SAM could be a 12-hole or 15-hole mask with a smaller total transmission but a better coverage of the frequency plane of the transfer function enabling image reconstruction for more complex objects.

3. PERFORMANCE STUDY

The performance of the high contrast modes depends on the residual aberrations after the Adaptive Optics system (AO). To evaluate the exoplanet detection capabilities of MICADO, we developed a dedicated simulation tool that uses the output of MICADO single conjugated AO simulation [2]. The key components of this simulator are outlined as follows:

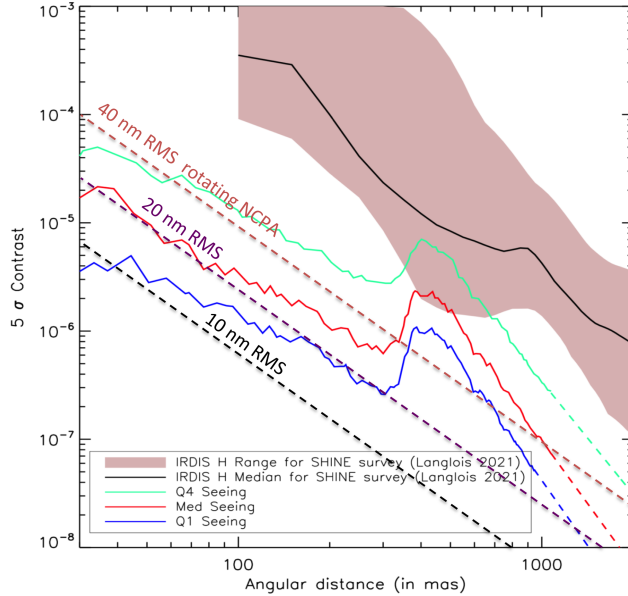
- The residual dynamical phase aberrations are calculated using a dedicated COMPASS simulation for 3 atmospheric seeing conditions with the 2 extrema of the 4 quartiles of seeing distribution given by ESO (Q1 and Q4) and the median one. They correspond to seeing computed at 30° of zenith of 0.49", 0.7", 1.19" for Q1, Median and Q4 respectively. The AO system simulated is a pyramid with a frequency of 500Hz [12].
- The simulation takes into account missing segments on the primary mirror, aberrations at different positions in the optical train (at the segment level, upstream and downstream of the coronagraph). These aberrations can be either static or varying. The simulator tool includes the different CLC and vAPP coronagraphs
- Other inputs of the simulator are the declination of the star (to calculate parallactic rotation and atmospheric refraction), the total observation time (typically 30 minutes crossing the meridian), star magnitude, planet spectrum. The simulation also takes into account photon noise for a given magnitude, detector readout noise and atmospheric emission. Different astrophysical scenes can be simulated: planets, disks.
- Post-processing is included in the performance analysis using classical Angular Differential Imaging (ADI).

In Figure 4, we present a typical 5σ contrast curve using the following assumptions:

- CLC1 (25 mas radius) without Non Common Path Aberrations (NCPA) except segments aberrations and 5 missing segments
- the 3 atmospheric seeing conditions described above
- 30 minutes observations around the transit of the star giving a parallactic angle variation of 20 deg (minimum zenith distance = 20°)
- H-short ($\lambda_{cen}=1.582\mu\text{m}$, $\Delta\lambda=0.085\mu\text{m}$)
- Post processing technique using classical ADI
- No photon noise or readout noise (only speckle noise)

The curves shown in Figure 4 were simulated without NCPA except segment aberrations and missing segments because we find that the effects of static NCPA is negligible up to about 50-100 nm RMS, thanks to ADI post-processing. On the contrary, the effects of non-static NCPA cannot be removed by the post-processing algorithms based on ADI since the first hypothesis of this technique is the stability of the instrument response function. The worst-case scenario is the presence upstream of the coronagraph of an aberration that would rotate with the parallactic angle. In that case, all the speckles created by this aberration would mimic rotating planets. Thus, when applying ADI, we could not discriminate between such speckles and a planet. We simulated different levels of upstream rotating aberration screens introducing random phases with a Power Spectral Density decreasing as f^{-2} with f the spatial frequency of the defects. The contrast after ADI processing worsens very rapidly as the aberration level increases (Figure 4). For a median seeing, a rotating aberration screen of 20 nm RMS increases by a factor 2 the residual level.

However, in high contrast mode (pupil tracking), there should be no element that rotates at the speed of the parallactic angle in the SCAO WFS or between the WFS and the focal plane mask that is only separated to the WFS by the Dichroic and the cryostat window. The main source of non-static NCPA will come from tip-tilt drift between the visible SCAO WFS and the IR position of the star at the entrance of the MICADO cryostat. To correct this effect, we will use a dedicated algorithm to stabilize the star on the CLCs with 0.5 mas precision [4]. Thus, we hope to reach a level of non-static NCPA of less than 20 nm RMS overs 30 minutes observations.



1

Figure 4. Detection contrast level (5σ RMS) assuming ADI post-processing. Simulation hypotheses are given in the text. The curves are compared to typical SPHERE results obtained for hundreds of datasets [6]. AO corrected observations over 30 minutes (180 images). Rotating NCPA aberrations are drawn over the figures for 3 levels of NCPA (dashed lines).

Even accounting for large non-static NCPA, we can see in Figure 4 that MICADO will allow much better performance than SPHERE. The improvement is two-fold. On one side, achieving contrast of $5 \cdot 10^{-6}$ to $5 \cdot 10^{-5}$ at angular separation below 200 mas is unparalleled. On the other side, we should reach contrast of 10^{-7} at 1 arcsecond, which is more than 1 to 2 order of magnitude better than what is achievable today. Consequently, MICADO should enable the exploration for new planets within previously identified planetary systems. These planets may be located closer to their host stars or less massive than the ones already detected at larger distance.

The improvement in angular resolution will additionally expand the range of ages for observed planetary systems. This will be achieved by investigating more remote young star associations, spanning a distance of 100-150 parsecs, as well as studying more mature systems thanks to the improved sensitivity. The improvements in both angular resolution and sensitivity will also significantly advance the morphological and dynamical analysis of interactions between planets and their surrounding disks.

Furthermore, even if not described here, the simultaneous coverage of H and K bands in long-slit spectroscopy, at a resolution of 20 000, is ideally suited for refining the characterization of exoplanet atmospheres. This will be accomplished by mitigating systematic errors within the spectrum, leading to a more precise determination of their composition.

4. CONCLUSION

The high contrast imaging mode of MICADO includes focal plane and pupil plan coronagraphs, a series of Lyot stops and spectral filters, as well as two Sparse Aperture masks. Detailed simulations show that the estimated performance is very exciting as it will extend the search scope of SPHERE, enabling the detection of very young, massive planets located at shorter orbital distances (a few astronomical units) from nearby stars and in more distant star associations (within 100-150 parsecs). Additionally, the enhanced angular resolution and sensitivity of MICADO are expected to facilitate the characterization of distant debris disks beyond what SPHERE can achieve, while providing more detailed images of the nearest ones.

In the next step, we will refine our performance estimates with physical inputs on the targets to better calculate the expected signal-to-noise ratio and the spectral and/or physical information we can derive from the measurements.

ACKNOWLEDGMENTS

This work was supported by the Action Spécifique Haute Résolution Angulaire (ASHRA) of CNRS/INSU co-funded by CNES.

References

- [1] J. -L. Beuzit et al. “SPHERE: the exoplanet imager for the Very Large Telescope”. In: *A&A*, arXiv:1902.04080 (Feb. 2019), arXiv:1902.04080. arXiv: [1902.04080](https://arxiv.org/abs/1902.04080) [[astro-ph.IM](#)].
- [2] Y. Clénet et al. “MICADO SCAO: to be or not to be... in MAIT”. In: *Proceedings of Adaptive Optics for Extremely Large Telescopes (AO4ELT7)*. 2023.
- [3] D. S. Doelman et al. “Vector-apodizing phase plate coronagraph: design, current performance, and future development”. In: *Applied Optics* 60.19 (July 2021), p. D52. DOI: [10.1364/AO.422155](https://doi.org/10.1364/AO.422155). arXiv: [2104.11211](https://arxiv.org/abs/2104.11211) [[astro-ph.IM](#)].
- [4] E. Huby et al. “STARLOC: the star tracking algorithm for the MICADO Lyot coronagraphs”. In: *Proceedings of Adaptive Optics for Extremely Large Telescopes (AO4ELT7)*. 2023.
- [5] S. Lacour et al. “Sparse aperture masking at the VLT. I. Faint companion detection limits for the two debris disk stars HD 92945 and HD 141569”. In: *A&A* 532, A72 (Aug. 2011), A72. DOI: [10.1051/0004-6361/201116712](https://doi.org/10.1051/0004-6361/201116712). arXiv: [1107.1426](https://arxiv.org/abs/1107.1426) [[astro-ph.IM](#)].
- [6] M. Langlois et al. “The SPHERE infrared survey for exoplanets (SHINE). II. Observations, data reduction and analysis, detection performances, and initial results”. In: *A&A* 651, A71 (July 2021), A71. DOI: [10.1051/0004-6361/202039753](https://doi.org/10.1051/0004-6361/202039753). arXiv: [2103.03976](https://arxiv.org/abs/2103.03976) [[astro-ph.EP](#)].
- [7] B. Lyot. In: *C. R. Acad. Sci. Paris* 191 (1930), p. 834.
- [8] B. A. Macintosh et al. “The Gemini Planet Imager: from science to design to construction”. In: *Society of Photo-Optical Instrumentation Engineers (SPIE) Conference Series*. Vol. 7015. Society of Photo-Optical Instrumentation Engineers (SPIE) Conference Series. July 2008. DOI: [10.1117/12.788083](https://doi.org/10.1117/12.788083).
- [9] D. Mawet et al. “Annular Groove Phase Mask Coronagraph”. In: *ApJ* 633 (Nov. 2005), pp. 1191–1200. DOI: [10.1086/462409](https://doi.org/10.1086/462409).
- [10] C. Perrot et al. “Design study and first performance simulation of the ELT/MICADO focal plane coronagraphs”. In: *Proceedings of Adaptive Optics for Extremely Large Telescopes (AO4ELT5)*. Apr. 2018, p. 159.
- [11] F. Snik et al. “The vector-APP: a broadband apodizing phase plate that yields complementary PSFs”. In: *Modern Technologies in Space- and Ground-based Telescopes and Instrumentation II*. Vol. 8450. Society of Photo-Optical Instrumentation Engineers (SPIE) Conference Series. Sept. 2012, 84500M, p. 84500M. DOI: [10.1117/12.926222](https://doi.org/10.1117/12.926222). arXiv: [1207.2970](https://arxiv.org/abs/1207.2970) [[astro-ph.IM](#)].
- [12] F. Vidal et al. “End-to-End simulations for the MICADO-MAORY SCAO mode”. In: *Proceedings of Adaptive Optics for Extremely Large Telescopes (AO4ELT5)*. Apr. 2018, 43, p. 43. DOI: [10.26698/AO4ELT5.0043](https://doi.org/10.26698/AO4ELT5.0043).